Submitted to
9/30/98

ESTIMATING SUBCANOPY SOIL MOISTURE WITH RADAR

Mahta Moghaddam and Sasan Saatchi
Jet Propulsion Laboratory, California Institute of Technology
Pasadena, CA 91109

Richard H. Cuenca
Bioresource Engineering Department
Oregon State University
Corvallis, OR 97331

ABSTRACT

The subcanopy soil moisture of a boreal old jack pine forest is estimated using polarimetric L- and P-band AIRSAR data. Model simulations have shown that for this stand, the principal scattering mechanism responsible for radar backscatter is the double-bounce mechanism between the tree trunks and the ground. The data to be used here were acquired during five flights from June to September 1994 as part of the BOREAS project. The dielectric constants, or equivalently moisture contents, of the trunks and soil can change significantly during this period. To estimate these dynamic unknowns, parametric models of radar backscatter for the double-bounce mechanism are developed using a series of simulations of a numerical forest scattering model. A nonlinear optimization procedure is used to estimate the dielectric constants. Ground measurements of soil and trunk moisture content are used to validate the results. The trunk moisture content measurements are very limited, but are used to gain confidence that the respective estimation results are accurate enough not to corrupt the soil moisture estimation, which is the main focus of this paper. After conversion of the trunk moisture measurements to dielectric constants, it is found that the estimated values are within 14% of the measurements. Due to potential calibration errors in the soil moisture measurements on the ground as well as in AIRSAR data, the variations rather than the absolute levels of the estimated soil moisture are considered. The results indicate that the estimated *variations* closely track the measurements. The worst case average estimated *change* differs by less than 1% volumetric soil moisture from that measured on the ground.

1. INTRODUCTION

The boreal ecosystem atmosphere study (BOREAS) project is a multidisciplinary effort to study the interactions between the boreal forest biome and the atmosphere to determine their role in global change. BOREAS is focused on two principle study areas in central Canada, one near the Prince Albert National Park in Saskatchewan, or the Southern study area (SSA), and the other near Thompson, Manitoba, or the Northern study area (NSA). Several intensive and focused field campaigns were carried out from April 1994 to September 1994, in which several remote sensing instruments made measurements. In particular,

the NASA/JPL airborne synthetic aperture radar (AIRSAR) collected polarimetric C-, L-, and P-band data during several flights in this time period. In this work, the focus is on the data acquired over an old jack pine (OJP) stand in the SSA. The SSA contains several conifer forest types such as young and old jack pine and black spruce. There are also deciduous species such as aspen, as well as stands consisting of mixtures of these species.

A major goal of remote sensing activities in BOREAS, such as radar measurements with the AIRSAR, was to retrieve forest parameters that play significant roles in the functioning of the ecosystem. Previously, we have reported an algorithm to estimate the tree canopy moisture content for a young jack pine stand in the BOREAS SSA from AIRSAR data [Moghaddam and Saatchi, 1998]. Another important parameter is soil moisture under the forest canopy. Soil moisture content can play a critical role in partitioning the energy balance latent and sensible heat fluxes, on plant water stress, and in the growth rate of forests. Numerous studies have shown the importance of correct soil moisture values for accurate simulation of processes in the atmospheric boundary layer [Cuenca et al, 1996].

In this work, an estimation algorithm is developed to obtain the soil moisture under an old jack pine stand for five different dates in the spring and summer of 1994. The structure of this stand enables a simplified modeling of the scattering process as described below. The extension of this algorithm to other stand types is currently under investigation and will be reported in future papers. As shown in Moghaddam and Saatchi [1995], double-bounce mechanism between the trunks and the ground is the scattering mechanism almost entirely responsible for the backscattered signal over the OJP site for the HH polarization at L- and P-bands (L-HH and P-HH) and the VV polarization at P-band (P-VV). For L-VV, the branch-ground interactions also become significant. The canopy's architecture varies on much longer time scales than its water content and the moisture content of soil. Therefore, it was assumed that parameters describing the geometry of trunks, branches, leaves, and soil are constant and known for the time period spanned by the AIRSAR data used in this paper. A parametric scattering model is derived in terms of the dielectric constant of the trunks and the dielectric constant of soil, which directly determine the moisture content. The model is used in a nonlinear algorithm to estimate the two dielectric constant values from P-HH, P-VV, and L-HH AIRSAR data.

An important question that arises in estimating soil moisture content is what is the depth of penetration of radar signals, or at what depth is the radar-estimated soil moisture content? The answer is highly dependent on the frequency and the value of the soil moisture content (dielectric constant). For dry soil which has a very low dielectric constant, penetration depths could exceed 1 m at L- and P-bands, whereas for high moisture contents, the radar signals penetrate to no more than a few centimeters. Here, we find that the dry sandy soil of the OJP allows deep (about 1 m) penetration of the L- and P-band signals. But even with higher moisture values and shallower radar penetration, it is possible to use the knowledge of soil moisture content at the surface and model its variations at larger depths [Camillo and Schmugge, 1983; Entekhabi et al., 1994].

Although in this work the soil and trunk dielectric constants are derived simultaneously, the results for soil are emphasized in more detail. The existing ground measurements for the dielectric constant of trunks are limited both in time and space, but are nonetheless used as a preliminary validation of the corresponding estimation results. For soil, after converting the dielectric constant to volumetric moisture content, comparisons of the results with available ground measurements are performed and good agreement is observed. The soil moisture measurements are available on a small spatial scale but an almost-continuous time period for the 1994 summer field campaigns. The local measurements result in limited validation of the radar-derived results, but this ultimately shows the strength of remote sensing data: if local measurements of a parameter can be used to validate the remote sensing techniques and algorithms, those data could be used to generate maps of that parameter over larger regional scales.

2. SITE DESCRIPTION

The old jack pine stand is one of the five main flux tower sites in the BOREAS Southern study area (SSA). It is characterized by tall trunks, a sparse crown layer, a "smooth" floor covered by lichen, and gentle topography. The average age of trees is 65 years. The soil is coarse sandy with low water holding capacity. Stand parameters which were directly measured by our group (BOREAS Remote Sensing Science RSS-16) during the 1994 summer, some through destructive sampling, are given in Table 1.

3. AIRSAR DATA

NASA/JPL AIRSAR data from several dates in the summer of 1994 were used to estimate the soil moisture and assess its changes at the OJP site. The specific dates were June 11, July 23, 25, and 28, and September 20. The AIRSAR collected fully polarimetric (HH, VV, HV, and VH) data at C-, L-, and P-bands, simultaneously. The aircraft track angle for all of the above flights was 341 degrees with respect to true North. The transmit bandwidth for all bands was 20 MHz, resulting in a range pixel spacing of 6.7 m and the cross-track swath width of 17 km. The incidence angles across the swath ranged from 25 degrees to 73 degrees, with the OJP stand being illuminated at an angle of about 45 degrees for all the data takes. Figure 1 shows the image obtained on July 23, 1994, which is a red-green-blue (RGB) overlay of the normalized total power for P-, L-, and C-bands, respectively. The OJP stand is outlined in white. The area near the BOREAS flux tower, where the ground measurements were performed, is marked with red within the larger OJP stand.

3.1. Scattering Mechanisms

The total radar backscattering cross section from a forested area in general consists of contributions from the crown layer volume scattering, trunk-ground double-bounce scattering, branch-ground double-bounce scattering, and surface scattering from the forest floor. Depending on the frequency, polarization, and canopy characteristics, one or more of the above mechanisms may be significant. It was shown in a previous paper [Moghaddam and Saatchi, 1995] that for the old jack pine stand, the radar backscatter is almost entirly dominated by the trunk-ground double-bounce mechannism at P-HH, P-VV, and L-HH. Although the L-VV backscattered signal is also predominantly characterized as double-bounce, it includes significant contribution from branch-ground scattering. The C-band backscatter for the OJP primarily consists of crown layer volume scattering. For all frequencies, the direct ground contribution is rather small. The backscatter channels most suitable for estimating subcanopy soil moisture, therefore, are P-HH, P-VV, and L-HH. The dominance of trunk-ground double-bounce scattering at low frequencies is not unique to this OJP stand, but can be observed in many other boreal zone forests, where there is a sparse crown layer and a dry ground cover or understory. An example would be spruce stands without a prominent moss ground cover. Therefore, although the estimation

method presented here is demonstrated for the OJP stand in the BOREAS SSA, it is not limited to this stand and can be easily applied to other stands with similar characteristics.

4. Soil Moisture Measurements

Soil moisture data were obtained by the HYD-1 group of BOREAS, which is one of the hydrology science groups with the goal of monitoring and collecting data on soil properties [BOREAS Information System(BORIS)]. Measurements were performed at the OJP site every other day during the 1994 intensive field campaigns (IFCs) in June, July, and September. A neutron probe was used and soil moisture was measured to a depth of 1.7 meters in 10 cm vertical intervals starting at a depth of 5 cm. The method of Parkes and Siam [1979] was applied to correct for the effects of neutron escape in the shallower depth layers. The measurements were performed along a transect line N 60 E (true) from the OJP flux tower at distances of 55 m, 65 m, 75 m, 85 m, and 105 m from the tower. As a quality control procedure, considering the Gaussian distribution of neutron emissions, two counts of backscattered neutrons were taken at each depth layer. If the two counts agreed to within 100, the average value was used in the probe calibratin equation. If not, the procedure was repeated until there were two values within 100 which were retained to compute soil moisture content. This procedure resulted in very stable values of soil moisture with minimal scatter due to instrument error [Vandervaere et al, 1994; Cuenca et al, 1997]. The data are used later in this paper to compare to the SAR-estimated values.

The major possible source of error for the neutron probe is calibration. Based on comparing to other methods of measurement, it is believed that the absolute error could be within $\pm 2\%$. However, there is high confidence in the change in moisture content from day to day.

5. ESTIMATION ALGORITHM

A two-step procedure is used to estimate soil dielectric constant ϵ_s, or equivalently, soil moisture, and trunk dielectric constant ϵ_t, from AIRSAR data. We have previously developed the underlying technique and applied it to the estimation of canopy moisture [Moghaddam and Saatchi, 1998] using the volume scattering mechanism. Here, we adapt

it to the case of trunk-ground double-bounce scattering. The algorithm can be summarized as follows:

1. *Parametric scattering model for the trunk-ground scattering mechanism*

The observation that the backscattered signal is almost completely due to ground-trunk double-bounce is key in formulating the parametric scattering model. From a numerical forest scattering model [Durden et al., 1989], synthetic data in the form of families of curves with the real parts of the dielectric constants of soil and tree trunks as the independent parameters are generated. Model simulations are shown in Figure 2(a)-(c). The parametric model is derived by fitting two-dimensional polynomials to the curves shown. For each frequency f and polarization PQ, the polynomial describing the radar backscatter σ_f^{PQ} can be written as

$$\sigma_f^{PQ} = \Sigma_{i_2=1}^{N_2} \left[\Sigma_{i_1=1}^{N_1} a_{i_1 i_2}^{PQ} \epsilon_t^{(i_1-1)} \right] \epsilon_s^{(i_2-1)}, \tag{1}$$

where ϵ_t is the relative dielectric constant of trunks, ϵ_s is the relative dielectric constant of soil, and the $a_{i_1 i_2}^{PQ}$ coefficients are calculated from the synthetic data. In this case, due to the smoothness and slow variations of the backscattered signals as shown, it was found that polynomials of third order, i.e., $N_1 = N_2 = 3$, are sufficient to achieve fitting errors of less than 1%.

In the numerical scattering model, the trunks are modeled as dielectric cylinders, and their interaction with the forest floor is modeled by multiplying their scattering matrix elements by the ground surface Fresnel reflection coefficients modified by the multiplicative factor

$$\exp(-2H^2 k_0^2 \cos^2 \theta_i),$$

where H is the rms surface height, k_0 is the free space wavenumber, and θ_i is the incidence angle. The effect of canopy attenuation is also taken into account. The model is explained in more detail in Durden at al. [1989]. It is assumed that the parameters describing the canopy geometry are known and fixed for the time period under study.

Since the dielectric constants are complex, there are generally four unknowns to estimate assuming they are frequency-independent (discussed further below). However, there are only three data channels that satisfy the criterion for "pure" trunk-ground mechanism. Furthermore, to improve the performance of the estimation algorithm in the presence of noise and calibration errors, it is desirable to allow the estimation problem to be over-determined, i.e., estimate no more than two parameters from the three data channels. This can be acheived by noting that the real and imaginary parts of the dielectric constant are related. It can be shown that the value of either the real or the imaginary part of the dielectric constant at any frequency can be determined if the other is known at all frequencies [Bohren and Huffman, 1983]. The relationships and constraints imposed on the relative values of the real and imaginary parts of the dielectric constant have also been studied from empirical and semiempirical perspectives [El-Rayes and Ulaby, 1987; Hallikainen et al., 1985; Klein and Swift, 1977; Mätzler, 1994; Oh et al. 1992].

Of particular relevance to the present work are the results reported in [Peplinski et al., 1995], where several measurements of the complex dielectric constant are performed for various types of soil over the frequency range 0.3 to 1.3 GHz, which includes the L- and P-band frequencies of the AIRSAR. Soil mixtures with various sand, silt, and clay content are considered. The same work will also be used later for relating the dielectric constant of soil to its moisture content. Based on the data shown in Peplinski et al. [1995], the real part of the soil dielectric constant for sandy soil does not change significantly in the frequency range considered. Furthermore, the real and imaginary parts of ϵ_s show an almost linear relationship in that frequency range, with a slope that is proportional to frequency. The data indicate that at 0.3 GHz, $\mathrm{Re}[\epsilon_s]/\mathrm{Im}[\epsilon_s] \approx 4.5$, and at 1.3 GHz, $\mathrm{Re}[\epsilon_s]/\mathrm{Im}[\epsilon_s] \approx 19$. Note that these factors are merely empirical approximations from measured data and not based on any rigorous derivation. Interpolating, we get $\mathrm{Re}[\epsilon_s]/\mathrm{Im}[\epsilon_s] \approx 6.5$ for P-band (0.44 GHz) and $\mathrm{Re}[\epsilon_s]/\mathrm{Im}[\epsilon_s] \approx 18$ for L-band (1.25 GHz). These linear relationships are used as a convenient approximation to reduce the number of independent parameters when generating the parametric scattering models. Since the imaginary part of the soil dielectric constant is much smaller than the real part, sometimes it is assumed that it can be ignored and set to zero. Although this is another way of reducing the number of unknowns, it will introduce larger errors and should be avoided unless alternate information is not available.

Similar relationships are used for the dielectric constant of trunks. To our knowledge, no extensive measurements of the complex ϵ_t for jack pine trees in the frequency range of interest are available. A few dielectric constant measurements were performed for the OJP site concurrently with the radar data acquisition on July 23 by one of the BOREAS remote sensing science teams, but the data are not yet available. Instead, we use the dielectric constant values reported in Saatchi and McDonald [1997] for this stand, which were obtained by using moisture content values furnished by destructive sampling of the OJP trees by the BOREAS Terrestrial Ecology group TE-6 [BOREAS Information System] and expressions derived by Ulaby and El-Rayes [1987] for converting vegetation moisture content to dielectric constant. These are reported in Table 2.

These values confirm our assumption that the trunk dielectric constants do not vary significantly between L- and P-bands (8% difference in the real part). The values in Table 2 represent the average dielectric constant of trunks and do not contain information about their profile as a function of radial distance into the trunk. The resulting approximate ratio of the real and imaginary parts of the trunk dielectric constant is $\mathrm{Re}[\epsilon_t]/\mathrm{Im}[\epsilon_t] \approx 4$.

2. *Nonlinear estimation algorithm to find the best set of unknowns that describes the SAR data given the parametric model.*

The parameter estimates are obtained by defining a least squares criterion based on minimizing the distance between data and model calculations given some a priori estimate of the parameters. It is carried out in an iterative fashion, each time updating the solution for the unknowns until an acceptably small error is reached. Let us denote the nonlinear model of scattering by $\mathbf{f}(\mathbf{X})$, where $\mathbf{X}$ is the vector containing the unknown parameters and $\mathbf{f}$ is a nonlinear functional of $\mathbf{X}$. The elements of $\mathbf{X}$ are the real parts of the soil and trunk dielectric constants in this case. Further, let $\mathbf{d}_{meas}$ be the vector of SAR measured data that contains the magnitude of P-HH, P-VV, and L-HH. The inverse problem can be stated as the problem of finding $\mathbf{X}$ such that $\mathbf{f}(\mathbf{X})$ and $\mathbf{d}_{meas}$ are "close," given some possible a priori knowledge of the unknowns. Equivalently, an $\mathbf{X}$ must be found such that a least-squares measure $\mathbf{L}(\mathbf{X})$ given by

$$\mathbf{L}(\mathbf{X}) = \frac{1}{2}\left\{ \|\mathbf{f}(\mathbf{X}) - \mathbf{d}_{meas}\|^2 + \|\mathbf{X} - \mathbf{X}_{ap}\|^2 \right\} \tag{2}$$

is minimized. Here, $\|\cdot\|$ denotes the L_2 norm, and $\mathbf{X}_{ap}$ is an a priori estimate of $\mathbf{X}$, which could be arbitrarily different from the true solution for $\mathbf{X}$.

The stochastic properties of data and unknowns were represented by applying their respective covariances when defining the L_2 norms:

$$\|\mathbf{f}(\mathbf{X}) - \mathbf{d}_{meas}\|^2 = (\mathbf{f}(\mathbf{X}) - \mathbf{d}_{meas})^t \cdot \overline{\mathbf{C}}_d^{-1} \cdot (\mathbf{f}_{nl}(\mathbf{X}) - \mathbf{d}_{meas}), \tag{3}$$

$$\|\mathbf{X} - \mathbf{X}_{ap}\|^2 = (\mathbf{X} - \mathbf{X}_{ap})^t \cdot \overline{\mathbf{C}}_{X_{ap}}^{-1} \cdot (\mathbf{X} - \mathbf{X}_{ap}), \tag{4}$$

where $\overline{\mathbf{C}}_d$ and $\overline{\mathbf{C}}_{X_{ap}}$ are data and a priori estimate covariance operators, respectively. The data covariance operator represents the statistics of the data including noise. It can be thought of as a measure of "closeness" of $\mathbf{d}_{meas}$ to $\mathbf{f}$. Similarly, $\overline{\mathbf{C}}_{X_{ap}}$ includes a priori information about the statistics of unknown parameters, and is also a measure of reliability of the a priori estimates [Tarantola, 1984]. If a reliable X_{ap} is not available, the elements of $\overline{\mathbf{C}}_{X_{ap}}$ are large so as to minimize the term $\|\mathbf{X} - \mathbf{X}_{ap}\|^2$ in Equation (2). The unknowns can be found by carrying out the following steps in an iterative fashion:

(a) Obtain an initial estimate for $\mathbf{X}$. This is $\mathbf{X}_{ap}$, and can be found either from previous measurements of $\mathbf{X}$, or by simply assigning an arbitrary value to it.

(b) Calculate an estimate of the data by using the latest estimate of $\mathbf{X}$, i.e., find $\mathbf{f}(\mathbf{X})$.

(c) Find $\mathbf{L}(\mathbf{X})$. This assumes knowledge of the covariance operators. The covariance operator $\overline{\mathbf{C}}_d$ can be calculated from the SAR data directly. It is generally assumed that the data channels are statistically independent. Therefore, $\overline{\mathbf{C}}_d$ is a diagonal matrix whose elements are simply the data variances associated with each channel within the group of pixels considered. The elements of the covariance matrix $\overline{\mathbf{C}}_{X_{ap}}$ are determined from a priori knowledge of the unknowns as mentioned above. If

L is small enough, the solution has been found; terminate the iterations. Continue otherwise.

(d) Find the direction of update for **X**.

(e) Find the step length in the direction of update.

(f) Update the solution to **X** by moving in the direction found in (d) by the length found in (e).

(g) Go to step (b).

We have used a preconditioned conjugate gradient method in steps (d) and (e) which has an improved convergence behavior over the conventional conjugate gradient solution. A more detailed explanation of the estimation algorithm can be found in Tarantola [1984].

6. RESULTS AND DISCUSSION

6.1. Estimated Moisture Variations

The algorithm described above was applied to AIRSAR data collected on June 11, July 23, July 25, July 28, and September 20, 1994. Figures 3(a)-(e) show maps of the estimated real part of the dielectric constant of trunks and Figures 4(a)-(e) the estimated real part of the dielectric constant of soil under the OJP canopy. The areas other than the old jack pine stands have been masked out, since the assumption of ground-trunk scattering and hence the estimation algorithm may not be valid there. The radar incidence angle at the OJP stand for all dates is 45-degrees. Each pixel in these figures is obtained by applying the estimation algorithm to a 5-pixel $\times$ 5-pixel box of the original image, which reduces the speckle effect.

The results of Figure 3 are summarized in Figure 5 for the area in the OJP stand near the BOREAS flux tower where the ground measurements were performed (red box in Figure 1). The error bars indicate the standard deviation of the estimated values about the mean estimated value for the outlined area. As expected, it is observed that the

dielectric constant, and hence moisture content, of the tree trunks stayed quite stable during the July data takes, while the longer-term behavior shows a slight decrease from June to September. Due to lack of more ground-truth data, it is only possible to compare the results with those in Table 2. This is not unreasonable, since the trunk moisture contents are not expected to change significantly during the growing season. The worst case difference between the average estimated and measured dielectric constants (real part) is 3.5, or about 14%. Unfortunately, further validation of trunk dielectric constants is not possible due to lack of more ground measurements. But this limited test at least gives us confirmation that the estimation accuracy for this parameter is high enough so as not to corrupt the soil moisture estimation results.

The real part of the dielectric constant of soil for the flux tower area is shown in Figure 6 for the five dates, again showing the shorter- and longer-term variations. The error bars represent the standard deviation of the estimated values about the mean estimated value. Using the semiempirical results of Peplinski et al. [1995] to relate dielectric constant to soil moisture, and noting that the soil in the OJP area consists of 92-98% coarse sand, we can obtain estimates of soil moisture. The formulas for conversion between soil moisture and dielectric constant are given explicitly in that reference and will not be repeated here. The results are given in the next subsection.

6.2. Comparison of Estimated Soil Moisture with Ground Measurements

The measured variations in soil moisture for June, July, and September 1994 for various depths are shown in Figure 7. The estimated values, converted from Figure 6, are superimposed for comparison. Regardless of the degree of agreement of the absolute estimated values with the measured ones, we will compare the levels of change of soil moisture. There are three reasons for doing so:

(1) The absolute soil moisture measured by the neutron probe may not be accurate, but the difference between the measurements from two dates should be highly accurate. This is due to possible calibration errors [Vandervaere et al., 1994].

(2) The calibration of AIRSAR data may contain systematic errors.

(3) The empirical formulas used to convert dielectric constant to soil moisture may not be accurate for the sandy OJP soil, but any systematic error is removed when the change in moisture for the same area at different times is considered.

The estimated and measured values are given in Table 3(a). The measured data are averaged over the five sample locations along the N 60 E (true) transect line and shown for various depths. The changes between each consecutive two dates are shown in Table 3(b). In June, the AIRSAR flight date was the 11th, whereas the neutron probe measurments were taken on the even dates. Therefore, the measurements from June 10th and 12th were linearly interpolated to appproximate that for June 11th. In July, the AIRSAR flew on the 23rd, 25th, and the 28th. The neutron probe measurments were taken on July 23rd, 25th, 27th, and 29th. The measurements from the 27th and 29th were interpolated to appproximate those for July 28th. Similarly for the September data, the last days of the neutron probe measurements were September 13th, 15th, and 18th, whereas the AIRSAR flight was on September 20th. The value used for comparison with the estimation result was that extrapolated from those last three dates.

To better understand how well the estimated soil moisture variations agree with the ground truth, the penetration depth of the electromagnetic waves into the soil must be investigated.

6.3. Depth of Penetration of Radar Signals

The electromagnetic waves reaching the forest floor can travel into the soil by a distance that is determined by the dielectric constant and frequency. Assuming the wave incident on the soil surface is a plane wave, and that the subsurface can be approximated by an effective homogeneous half-space, the transmitted wave $E_{f,P}$ of frequency f and polarization P can be symbolically written as

$$E_{f,P} = A \exp(ikd), \tag{5}$$

where A is the amplitude of the transmitted wave at the surface, k is the wavenumber of the subsurface medium, and d is the distance into the ground. The wavenumber k is a

complex number given by

$$k = k_R + ik_I = 2\pi f\sqrt{\mu\epsilon_s}. \tag{6}$$

From Equations (5) and (6), as the signal travels a distance d, it is attenuated by the factor γ given by

$$\gamma = \exp(-k_I d). \tag{7}$$

The distance required for the wave to attenuate by $1/e$ is called the pentration depth:

$$d_{penetration} = 1/k_I. \tag{8}$$

From the real part of the dielectric constants estimated here and shown in Figure 6, the imaginary part and hence the penetration depth can be calculated, which could be over 1 m for both L- and P-bands, as shown in Table 4. For the dielectric constants estimated here, Table 4 shows the penetration depths for L- and P-bands. Note that the two frequencies have very similar penetration depths, which range from around 1m to around 1.3m depending on the moisture content.

The estimated dielectric constants can be thought of as average values from the soil surface down to the depth to which the radar signal can penetrate. In other words, the radar integrates the dielectric constant, or moisture, of the soil contained in the penetration depth. Therefore, the estimated soil moisture can be considered to be the average value within the penetration depth. We emphasize that this method does not yield the soil moisture profile, but rather its integrated value down to the depth of signal penetration. In this case, Table 3(b) can be rewritten as in Table 5, which indicates that in the worst case, variations are estimated to within 0.8% volumetric moisture content (last row in Table 5).

The results here indicate that it is possible to estimate soil moisture content down to a depth of over 1 m if the real part of the relative dielectric constant of soil is as low as about 2. However, note that this depth is highly dependent on the value of the dielectric constant, and hence can change considerably with changes in soil moisture content. If, for example, the soil dielectric constant increases after a precipitation event, the penetration depth would be considerably smaller. In such a case, the estimated value of the dielectric constant can be used again with Equation (8) to approximate the penetration depth. It has been shown that near-surface soil moisture values can be used to obtain the soil moisture profile at larger depths [Camillo and Schmugge, 1983; Entekhabi et al., 1994].

6.4. Extension to Other Forest Types

The OJP forest was considered due to its structural simplicity which results in a single-mechanism backscatter for the P-band and L-band channels considered. The technique used here is not limited to this stand, but can be used for any forest with characteristics manifested by the OJP, i.e., "tall" trunks, sparse branch layer, dry understory or ground cover, and a "smooth" floor. In fact, these characteristics are not uncommon in the boreal zone, where many dry conifer stands exist. Besides the old jack pines, spruce forests without moss are examples of potential candidates for this technique.

In the general case, however, scattering from a forest consists of several mixed mechanisms. It has been shown, e.g., in Moghaddam and Saatchi [1995], that different frequencies and polarizations are sensitive to different scattering mechanisms. In the case of AIRSAR therefore it is in principle possible to separate various mechanisms by studying all available data channels. For example, let us assume that for a certain forest stand the backscatter at P- and L-bands is a mixture of volume and double-bounce scattering, with only volume scattering significant at C-band. It might be possible to estimate parameters describing the branch-layer using volume scattering analysis on quad-pol C-band data [Moghaddam and Saatchi, 1998], use the information obtained in a theoretical model to calculate the volume scattering contribution at L- and P-bands, and remove it from the total measured radar backscatter at those frequencies. The remainder would be the double-bounce contribution, which can be used as was done in the present work to estimate trunk and soil moisture. A complete treatment of this problem is left for a future paper.

7. SUMMARY

The subcanopy soil moisture of a boreal old jack pine forest was estimated using polarimetric L- and P-band AIRSAR data. In particular, L-HH, P-HH, and P-VV channels were used. The OJP was one of the five flux tower sites in the BOREAS Southern study area. Five AIRSAR datasets from June to September 1994 were used to estimate the variations in soil and trunk moisture during this time period. To estimate these dynamic unknowns, parametric models of radar backscatter for the double-bounce mechanism were developed by using a series of simulations of a numerical forest scattering model. The resulting simulated data were used to derive polynomial fits of backscattering cross section as a function of the ground and trunk dielectric constants. Empirical and field data were used to relate the real and imaginary parts of the dielectric constants, and hence formulate the parametric model in terms of two unknowns only. A nonlinear optimization procedure was used to estimate the dielectric constants, and hence, in particular, soil moisture.

Ground measurements of soil and trunk moisture content were used to validate the results. The trunk moisture measurements are very limited. Hence, those results were not emphasized as much as soil moisture, but they still show that the trunk dielectric constant is estimated to within 14% of the measurments. To remove the effect of calibration errors in the soil moisture measurements on the ground, the variations, rather than the absolute levels, of the estimated soil moisture were considered. The results indicated that the radar is capable of monitoring subtle moisture variations, which differ less than 1% volumetric soil moisture from the measured values. The soil moisture results were validated on a small spatial scale due to lack of more extensive ground measurements, but show the strength of remote sensing in mapping parameters on large scales whereas manual ground measurements could reasonably be obtained only on a much more limited scale. This algorithm has the potential of being extended to other forest types with more complex combinations of scattering mechanisms by using other available SAR frequencies and polarizations.

ACKNOWLEDGMENT

This work was performed in part by the Jet Propulsion Laboratory, California Institute of Technology, under contract from the National Aeronautics and Space Administration.

REFERENCES

Bohren, C. F., and D. R. Huffman. *Absorption and Scattering of Light by Small Particles*, Wiley-Interscience, New York,1983..

BOREAS Information System (BORIS), online via the World-Wide Web, http://boreas.gsfc.nasa.gov/, 1994-1998.

Camillo, P. J., and T. J. Schmugge, Estimating soil moisture storage in the root zone from surface measurements. *Soil Sci., 135(4)*, 245–264, 1983.

Cuenca, R. H., M. Ek, and L. Mahrt, Impact of soil water property parametrization on atmospheric boundary-layer simulation. *J. Geophysic. Res., 101*, 7269–7277, 1996.

Cuenca, R. H., D. E. Stangel and S. F. Kelly, Soil water balance in a boreal forest, *Journal of Geophysical Research - BOREAS Special Issue, 102(D24)*, 29355–29365, 1997.

Durden, J. van Zyl, and H. Zebker, Modeling and observation of the radar polarimetric signature of forested areas. *IEEE Trans. Geosci. Remote Sensing, 27(3)*, 290–301,1989.

El-Rayes, M. A. and F. T. Ulaby, Microwave dielectric spectrum of vegetation – Part I: Experimental observations. *IEEE Trans. Geosci. Remote Sensing, 25(5)*, 541–549, 1987.

Entekhabi, D., H. Nakamura, and E. Njoku, Solving the inverse problem for soil moisture and temperature profiles by sequential assimilation of multifrequency remotely sensed observations. *IEEE Trans. Geosci. Remote Sensing, 32(2)*, 438–448, 1994.

Hallikainen, M. T., F. T. Ulaby, M. C. Dobson, M. A. El-Rayes, and L. K. Wu, Microwave dielectric behavior of wet soil - Part I: Empirical models and experimental observations. *IEEE Trans. Geosci. Remote Sensing, 23*, 25–34, 1985.

Klein, L. A., and C. T. Swift, An improved model for the dielectric constant of sea water at microwave frequencies. *IEEE Trans. Antennas Propagat., 25*, 104–111, 1977.

Mätzler, C., Microwave dielectric model of leaves. *IEEE Trans. Geosci. Remote Sensing,*

32(4), 947–949, 1994.

Moghaddam and S. Saatchi, Analysis of scattering mechanisms in SAR imagery over boreal forest: Results from BOREAS'93. *IEEE Trans. Geosci. Remote Sensing, 33(5)*, 1290–1296, 1995.

Moghaddam and S. Saatchi, Monitoring tree moisture using an inversion algorithm applied to SAR data. *IEEE Trans. Geosci. Remote Sensing*, in press, 1998.

Oh, Y., K. Sarabandi, and F. T. Ulaby, An empirical model and an inversion technique for radar scattering from bare soil surfaces. *IEEE Trans. Geosci. Remote Sensing, 30*, 370–381, 1992.

Peplinski, N. R., F. T. Ulaby, and M. C. Dobson, Dielectric properties of soils in the 0.3–1.3-GHz range. *IEEE Trans. Geosci. Remote Sensing, 33(3)*, 803–807, 1995.

Parkes, M. E. and N. Siam, Error associated with measurement of soil moisture change by neutron probe, *J. Agric. Eng. Res., 24(1)*, 87–93, 1979.

Saatchi, S., and K. C. McDonald, Coherent effects in microwave backscattering models for forest canopies. *IEEE Trans. Geosci. Remote Sensing, 35(4)*, 1032–1044, 1997.

Tarantola, A, The seismic reflection inverse problem, in *Inverse Problems of Acoustic and Elastic Waves*, F. Santosa, Y. H. Pao, W. Symes, and C. Holland, Eds., SIAM, Philadelphia, 1984.

Ulaby, F. T., and M. A. El-Rayes, Microwave dielectric spectrum of vegetation. *IEEE Trans. Goesci. Remote Sensing, 25*, 550–557, 1987.

Vandervaere, J-P., M. Vauclin, R. Haverkamp and R. H. Cuenca, Error analysis in estimating soil water balance of irrigated fields during the EFEDA experiemnt: 1. Local Standpoint. *J. Hydrology, 156*, 351–370, 1994.

Figure Captions

Figure 1. AIRSAR image obtained on July 23, 1994, which is a red-green-blue (RGB) overlay of the normalized total power for P-, L-, and C-bands, respectively. The OJP stand is outlined in white. The area near the BOREAS flux tower, where the ground measurements were performed, is marked with red within the larger OJP stand.

Figure 2. Simulations from a numerical forest scattering model [Durden et al., 1989], where synthetic data in the form of families of curves with the real parts of the dielectric constants of soil and tree trunks as the independent parameters are generated.

Figure 3. (a)-(e) Maps of the estimated real part of the dielectric constant of trunks. The areas other than the old jack pine stands have been masked out.

Figure 4. (a)-(e) Maps of the estimated real part of the dielectric constant of soil under the OJP canopy. The areas other than the old jack pine stands have been masked out.

Figure 5. Summary of the results of Figure 3 for the area in the OJP stand near the BOREAS flux tower where the ground measurements were performed (red box in Figure 1). The error bars indicate the standard deviation of the estimated values about the mean estimated value.

Figure 6. The real part of the dielectric constant of soil for the flux tower area for the five dates, showing the shorter- and longer-term variations.

Figure 7. The measured variations in soil moisture for June, July, and September 1994 for various depths, averaged over five sample locations. The estimated values, converted from Figure 6, are superimposed for comparison.

Table 1. OJP stand parameters from ground measurements.

Parameter	Value
tree density (#/m^2)	0.3
canopy thickness (m)	9.0
trunk height (m)	15.1±3.0
dbh (cm)	13.0±4.9
primary branch density (#/m^3)	7
primary branch orientation (degrees)	80
primary branch length (m)	0.7±0.18
primary branch diameter (cm)	1.0±0.21
secondary branch density (#/m^3)	70
secondary branch diameter (cm)	0.4±0.07
secondary branch length (m)	0.25±0.08
needle length (cm)	2.5±0.4
needle diameter (mm)	1.0
needle density (#/m^3)	1500
soil rms roughness (cm)	1.5

Table 2. Dielectric constant of OJP trunks from measured moisture content and Ulaby–El-Rayes expressions.

Date	L-band	P-band
June 1994	(23.1,6.2)	(26.3,6.1)

Table 3(a). Comparison of measured (denoted "probe") and estimated volumetric soil moisture values (%). All measured values are assumed to have ±2% error.

Date (dd/mm/yy)	Estimated	probe 5cm	probe 25cm	probe 45cm	probe 65cm	probe 85cm	probe 105cm	probe 125cm
11/06/94	6.4± 2.7	7.7	9.1	8.7	8.3	8.9	8.8	9.7
23/07/94	7.2± 2.8	9.3	9.6	9.1	8.7	9.3	9.5	10.6
25/07/94	6.5± 2.5	8.3	9.2	8.7	8.3	8.9	8.9	10.0
28/07/94	6.1± 2.8	7.5	8.8	8.5	8.1	8.6	8.5	9.9
20/09/94	3.5± 2.5	4.2	6.3	7.1	6.9	7.4	7.3	7.9

Table 3(b). Comparison of changes in mean volumetric soil moisture (%), derived from Table 3(a).

Dates (dd/mm/yy) Differenced	Estimated	probe 5cm	probe 25cm	probe 45cm	probe 65cm	probe 85cm	probe 105cm	prob 125cm
23/07/94-11/06/94	0.8	1.6	0.5	0.4	0.4	0.4	0.7	0.9
25/07/94-23/07/94	-0.7	-1.0	-0.4	-0.4	-0.4	-0.4	-0.6	-0.6
28/07/94-25/07/94	-0.4	-0.8	-0.4	-0.2	-0.2	-0.3	-0.4	-0.1
20/09/94-28/07/94	-2.6	-3.3	-2.5	-1.4	-1.2	-1.2	-1.2	-2.0

Table 4. Mean penetration depth for the estimated dielectric constants of soil. For 20/09/94, the lower value of the estimated dielectric constant was set to 1.0 to avoid a nonphysical situation.

Date (dd/mm/yy)	Estimated ϵ_s	$d_{penetration}$ (m), L-band	$d_{penetration}$ (m), P-band
11/06/94	1.78± 0.45	1.10	1.09
23/07/94	1.95± 0.58	1.02	1.01
25/07/94	1.81± 0.55	1.07	1.06
28/07/94	1.74± 0.56	1.15	1.15
20/09/94	1.22± 0.32	1.29	1.27

Table 5. Comparison of changes in mean volumetric soil moisture (%), derived from Table 3(b) by averaging over the penetration depths of Table 4.

Dates (dd/mm/yy) Differenced	Estimated	Probe
23/07/94-11/06/94	0.8	0.6
25/07/94-23/07/94	-0.7	-0.5
28/07/94-25/07/94	-0.4	-0.3
20/09/94-28/07/94	-2.6	-1.8

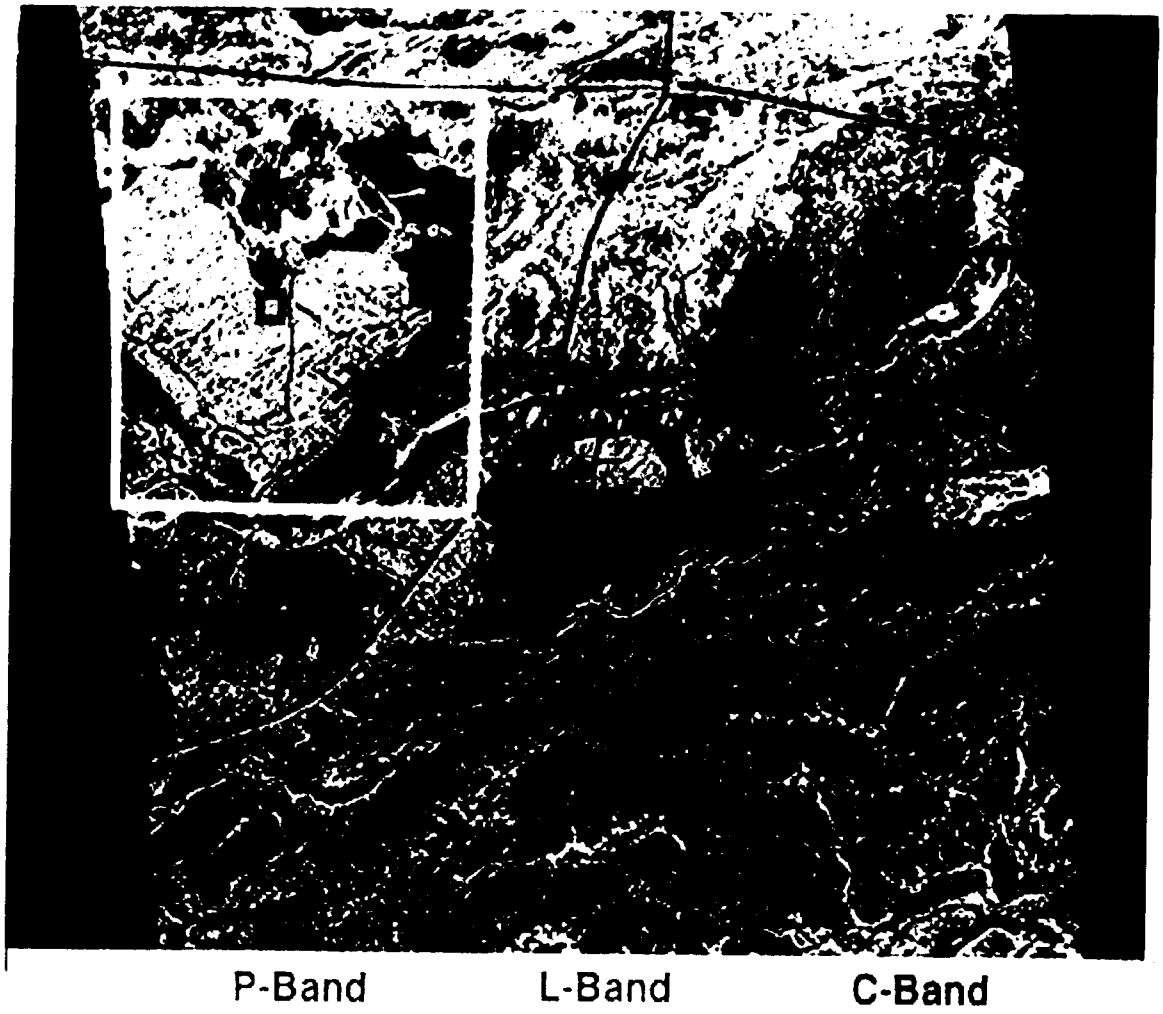

Figure (1)

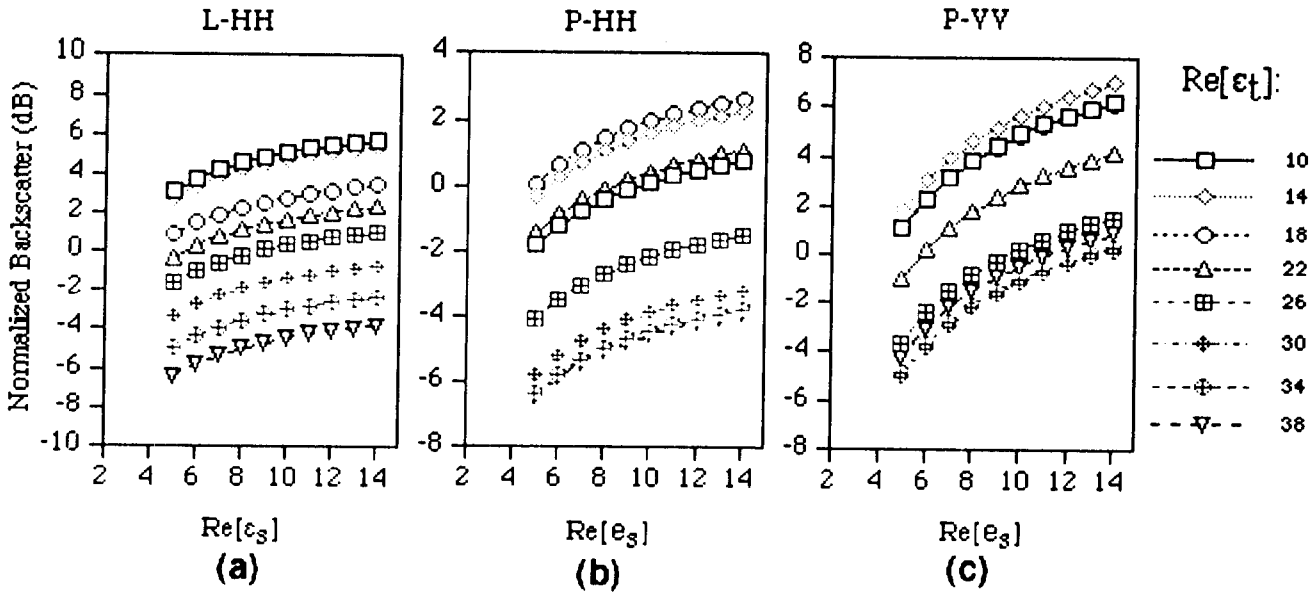

Figure (2)

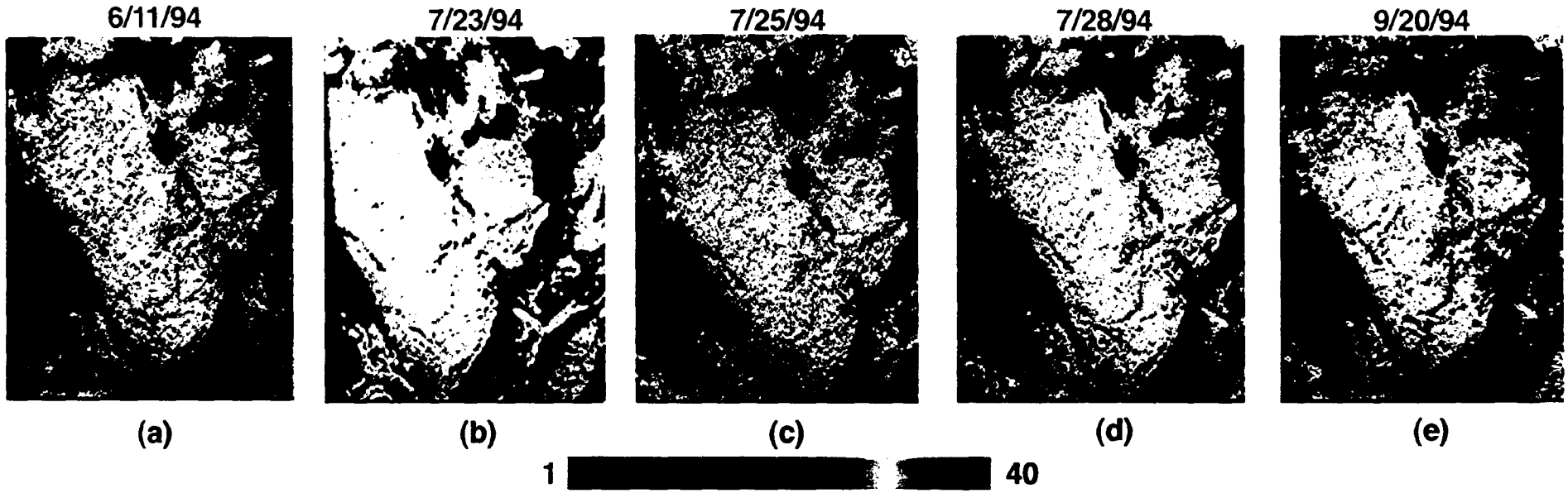

Figure 3. Variations of dielectric constant of OJP trunks

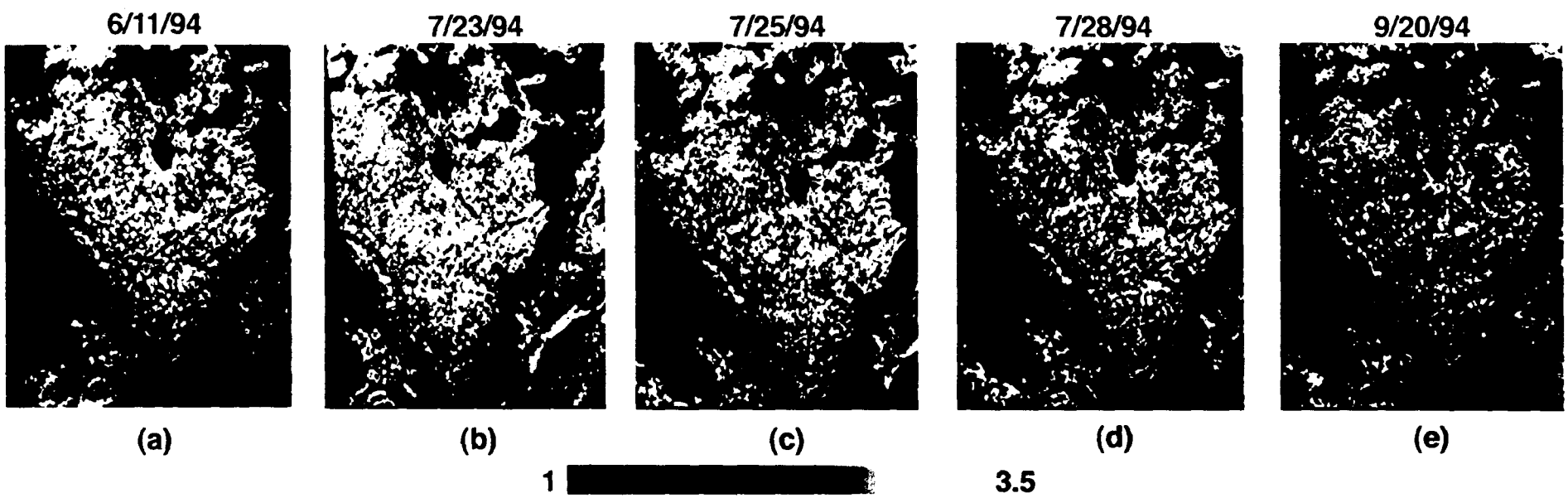

Figure 4. Variations of dielectric constant of soil

Variations in Real Part of Trunk Dielectric Constant

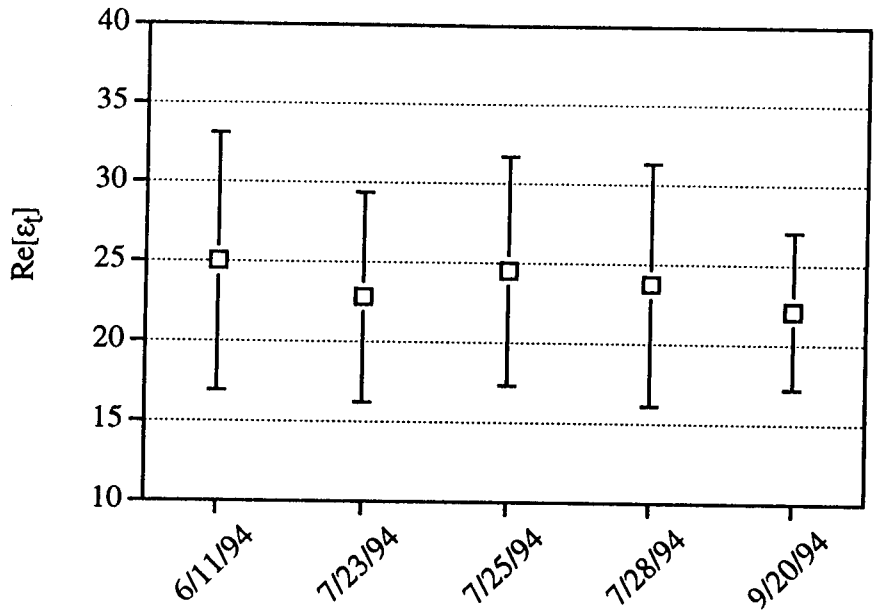

Figure 5

Variations in Real Part of Soil Dielectric Constant

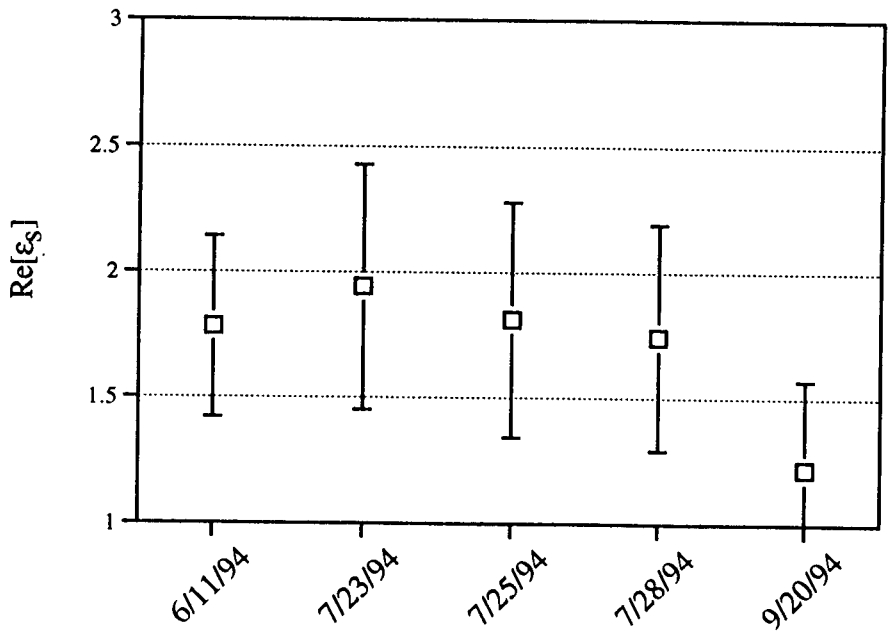

Figure 6

Measured and Estimated Volumetric Soil Moisture at OJP

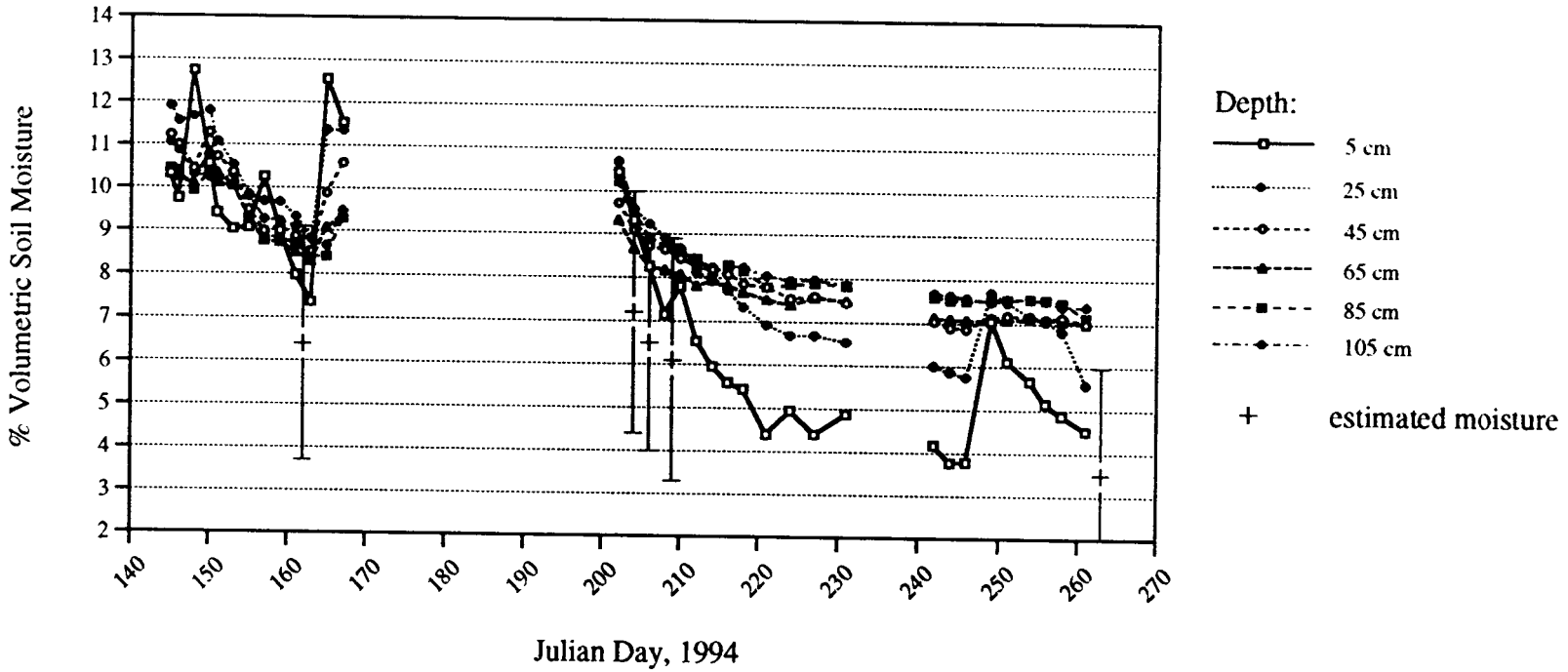

Figure 7